DOI: 10.21917/ijivp.2016.0199

AUTOMATED DETECTION OF MITOTIC FIGURES IN BREAST CANCER HISTOPATHOLOGY IMAGES USING GABOR FEATURES AND DEEP NEURAL NETWORKS

Maqlin Paramanandam[1], Robinson Thamburaj[2] and Joy John Mammen[3]

[1,2]*Department of Mathematics, Madras Christian College, India*

E-mail: [1]maqlinparamanandam@yahoo.com, [2]robinson@mcc.eud.in

[3]*Department of Transfusion Medicine, Christian Medical College Hospital, India*

E-mail: [3]joymammen@cmcvellore.ac.in

Abstract

The count of mitotic figures in Breast cancer histopathology slides is the most significant independent prognostic factor enabling determination of the proliferative activity of the tumor. In spite of the strict protocols followed, the mitotic counting activity suffers from subjectivity and considerable amount of observer variability despite being a laborious task. Interest in automated detection of mitotic figures has been rekindled with the advent of Whole Slide Scanners. Subsequently mitotic detection grand challenge contests have been held in recent years and several research methodologies developed by their participants. This paper proposes an efficient mitotic detection methodology for Hematoxylin and Eosin stained Breast cancer Histopathology Images using Gabor features and a Deep Belief Network- Deep Neural Network architecture (DBN-DNN). The proposed method has been evaluated on breast histopathology images from the publicly available dataset from MITOS contest held at the ICPR 2012 conference. It contains 226 mitoses annotated on 35 HPFs by several pathologists and 15 testing HPFs, yielding an F-measure of 0.74. In addition the said methodology was also tested on 3 slides from the MITOSIS- ATYPIA grand challenge held at the ICPR 2014 conference, an extension of MITOS containing 749 mitoses annotated on 1200 HPFs, by pathologists worldwide. This study has employed 3 slides (294 HPFs) from the MITOS-ATYPIA training dataset in its evaluation and the results showed F-measures 0.65, 0.72and 0.74 for each slide. The proposed method is fast and computationally simple yet its accuracy and specificity is comparable to the best winning methods of the aforementioned grand challenges.

Keywords:

Breast Cancer, Deep Neural Networks, Gabor Filter, Histopathology, Mitotic Count

1. INTRODUCTION

In Breast cancer pathology, the single factor that best aids in establishing the proliferative activity of the tumor is the number of cells undergoing mitotic division visible under a fixed number of high power fields (HPF - the area of tissue under the microscope set to a high magnification). Studies reveal that mitotic count is considered the most independent prognostic parameter that determines patient risk [1] and is assessed through the strictest of protocols. However, mitotic counting is highly subjective, prone to inter and intra observer variability [2]. An automated detection of mitotic figure using image analysis could be an efficient, error free and time saving also making results obtained by different pathologists comparable.

Automated mitotic detection has certain innate challenges due to the high-complexity in appearance. The most prominent feature of a cell undergoing mitotic division is its hyperchromaticity, and effective care needs to be taken to avoid counting other hyperchromatic elements such as lymphocytes or apoptic nuclei as mitoses. Another challenge is the variability in the shapes of mitosis in its four main phases: prophase, metaphase, anaphase and telophase shown in Fig.1(a-d) respectively. Specifically, a mitotic cell in telophase, though having two separate and fully divided nuclei, should be counted as a single mitotic figure. The Fig.1(e)-Fig.1(h) shows certain hyperchromatic nuclei which have close resemblance to mitotic figures.

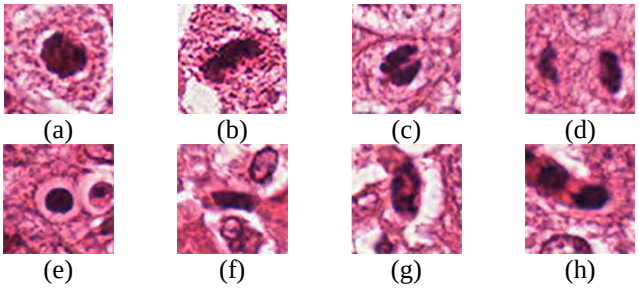

Fig.1. (a-d) Different phases of mitotic figures, (e-h) Other Hyperchromatic nuclei in the images which closely resemble mitotic figures

Given the significance of the Mitotic count and the related issues, this paper proposes an efficient mitotic detection methodology for H&E stained breast cancer histopathology images. From input breast cancer histopathology image the proposed method detects mitotic figures using automated image analysis and a trained Deep Belief Network - Deep Neural Network classifier (DBN-DNN). The method is trained and evaluated on breast histopathology images from dataset presented at MITOS contest held at ICPR 2012 conference [3] and MITOSIS- ATYPIA grand challenge held at ICPR 2014 [4].

The paper is organized as follows: Section 2 gives a short review of the related works. Section 3 describes the dataset and ground truth followed by a presentation of methodology in Section 4 and the results and concluding remarks are laid out in Section 5 and Section 6 respectively.

2. RELATED WORKS

Very little documentation on automated mitotic detection can be found, on research done two decades ago, owing to the fact that only limited computational and tissue digitization resources were available at the time. Recent interest was kindled after the advent and widespread usage of Whole Slide scanners [5], [6]. To help

matters further, the benchmark datasets of breast histopathology images annotated with mitotic figures were made publicly available at certain grand challenges and have spawned numerous approaches proposed by various authors [3], [7].

An efficient pixel classification application by supervised Deep Neural Networks [8] won the MITOS grand challenge of ICPR 2012 contest. The proposed DNN construction was a max-pooling (MP) convolution neural network (CNN) that operates on RGB pixels sampled from a square patch of the source image. Since the DNN operates on raw pixel values it learns a set of visual features from the training data without the need for human hand crafted features. It was proved to outperform all the other competing techniques. However the contests was held for a relatively small dataset (5 slides in total, 10 annotated HPFs per slide) and since regions of same slide were included in both training and testing set the issues related to inter-subject variability were not taken into consideration. These issues were addressed in the next contest, 'Assessment of algorithms for mitosis-detection in breast cancer histopathology images' AMIDA 2013.

The methods proposed in AMIDA 2013 [7] can be roughly categorized into two groups: 1. Methods involving candidate detection which are classified based on certain hand crafted features into mitoses or non-mitoses classes. 2. Pixel Classifiers that when directly applied to the image pixels tend to classify them into mitotic or non mitotic class. A vast majority of the methods belonged to the former group wherein candidate regions were obtained by applying thresholding or morphological operations to a grayscale images or mitosis probability maps. The features extracted from the candidate regions were used for the classification task. The winning method [8] belonged to the latter group and proved to be more powerful in mitotic detection. It presented an efficient implementation of deep convolution neural networks to obtain a mitosis probability map for each image, from which mitoses were detected by non-maxima suppression.

3. DATASET AND GROUND TRUTH

This section gives a brief description of datasets used in this paper. The proposed model has been trained and tested on the publicly available dataset of the MITOS contest and the training dataset of its extension MITOS-ATYPIA contest. From the MITOS-ATYPIA dataset, only the training portion is used in the study as the ground truth for test dataset has not yet been made public.

3.1 MITOS

It constitutes images from a set of 5 Hematoxylin and Eosin (H&E) stained breast cancer biopsy slides of different patients scanned by two different slide scanners: Aperio Scanscope XT and Hamamastu Nanozoomer 2.0-HT. In each slide, 10 HPFs were selected by two different pathologists. An HPF has a size of 512 $\mu m^2 \times 512$ μm^2 which is the equivalent of a microscope field diameter of 0.58 mm. These 50 HPFs contain a total of 326 mitoses. The training and testing set consisted of 35 and 15 HPFs containing 226 and 100 mitoses, respectively. Two different breast cancer oncologists have provided the ground truth for location of mitotic figures. Each image is accompanied by a CSV file containing the pixel locations of the manually segmented mitotic nuclei.

3.2 MITO-ATYPIA

The publicly available training dataset of MITOS-ATYPIA is used to evaluate the proposed framework. It constitutes images of a set of 1200 high power field at x40 magnification obtained from Hematoxylin and Eosin (H&E) stained breast cancer biopsy slides of 11 patients scanned by two different slide scanners: Aperio Scanscope XT and Hamamatsu Nanozoomer 2.0-HT. Each image frame at x40 magnification comes with two ground truth CSV files which indicate the approximate centre of each single mitotic figure or non mitotic figure. There are total of 1200 frames at x40 magnification. In this research work the dataset is divided into training and testing set consisting of 8 and 3 slides each having 928 and 294 high power fields respectively. A summary of the dataset used is provided in Table.1.

Table.1. Summary of datasets used for on the proposed method

Dataset/No of biopsy slides	Scanner	Resolution at x40	Dimensions	No. of HPFs /No of Mitotic figures
MITOS / 5 slides	Aperio Scanscope XT	0.2456 µm per pixel	1539 ×1376 pixels 377.824 × 337.808 μm^2	Training set - 35/226 Testing set - 15/100
	Hamamatsu Nanozoomer 2.0-HT	0.2273 µm per pixel (horizontal) 0.22753 µm per pixel (vertical)	1663 ×1485 pixels 377.998 × 337.883 μm^2	Training set- 35/226 Testing set- 15/100
MITOS-ATYPIA/ 11 slides	Aperio Scanscope XT	0.2455 µm per pixel	2084 × 2084 pixels	Training set- 928 /669 Testing set- 294/80
	Hamamatsu Nanozoomer 2.0-HT	0.227299 µm per pixel (horizontal) 0.227531 µm per pixel (vertical)	2252 × 2250 pixels	Training set- 928 /673 Testing set- 294/80

4. METHODOLOGY

The Fig.2 shows the step-wise graphical summary of the mitoses detection methodology. The methodology can be divided into a) Pre-processing, b) Candidate detection, c) Feature Extraction and d) Classification

4.1 CANDIDATES DETECTION

The most distinguishing feature of a mitotic cell is its hyperchromaticity. Given an input RGB image, the candidate detection aims at mapping a square window around every hyperchromatic dark object in the image that is possibly a mitotic cell. This is done in the following steps.

4.1.1 RGB to Gray using PCA:

Principal Component Analysis is used to find the primary axis in the RGB color space. This is done by computing the Eigen decomposition of the co-variance matrix of the three color channels. The Eigen vector that corresponds to the largest Eigen value is the primary axis along which the full resolution image is projected using closest point, i.e. the pixel values are multiplied by the Eigen vector that corresponds to the largest Eigen value. This results in a gray image. The gray image is normalized to range [0 1].

4.1.2 Gaussian Filter:

The gray image is then subject to a Gaussian low pass filtering [9] of size 5×5 and standard deviation 2.

4.1.3 Candidate Seed Location:

This is followed by an h-minima transformation of the gray image resulting in candidate seed points. Herein all regional minima in the image lesser than an *h*-value is removed. The image is then converted to a binary image by Otsu's thresholding. Each connected component of the image is a hyperchromatic object. The intensity weighted centroid of each connected component gives the location of the hyperchromatic dark objects in the image

4.1.4 Hyperchromatic Object Patch Extraction:

A square region of size 80×80 is centered on every candidate seed point. This step results in detecting all the mitotic figures and other hyperchromatic objects in the image.

4.1.5 Labeling the Patches as Mitotic and Non Mitotic:

As indicated in the MITOS ATYPIA contest's evaluation criteria, a detected candidate is labeled as a true mitotic figure if its distance is within 8 µm (~32 pixels) from the centre of a ground truth mitotic figure (given for training dataset of MITOS ATYPIA by pathologists). All the hyperchromatic objects other than mitotic figures are labeled as non-mitotic candidates. Since the number of mitotic figures is relatively small compared to the non-mitotic ones, and considering the fact that the mitotic detection problem is rotationally invariant, additional training instances of mitotic figures are generated by rotations and mirroring (*original mitotic figure* + 3 *types of rotations* + *horizontal flip* + *vertical flip* = 6 *instances of a mitotic figure*). In addition, the MITOS-ATYPIA dataset provides ground truth information for locating non-mitotic figures which closely resemble mitotic figures.

4.2 GABOR FEATURE EXTRACTION

Gabor filters [10][11] when convolved with images, give higher responses at texture changes which are crucial for discriminating mitotic cells from other hyperchromatic objects in the image. A Gabor feature vector is extracted by 2-D Gabor convolution [12] of each candidate image patches. A 2-D Gabor filter is a Gaussian kernel modulated by a sinusoidal plane wave defined by the equation,

$$g(x,y)=\frac{f}{\pi\gamma\eta}\exp\left(\frac{x^2+\gamma^2 y'^2}{2\sigma^2}\right)\exp\left(j2\pi f x'+\varphi\right) \qquad (1)$$

where, $x' = x\cos\theta + y\sin\theta$, $y' = -x\sin\theta + y\cos\theta$, f is the frequency of the sinusoid curve, γ is the spatial aspect ratio which specifies the elasticity of the support of the Gabor function, θ represents the orientation of the normal to the parallel stripes of the Gabor function, φ is the phase offset, σ is the standard deviation of the Gaussian envelop.

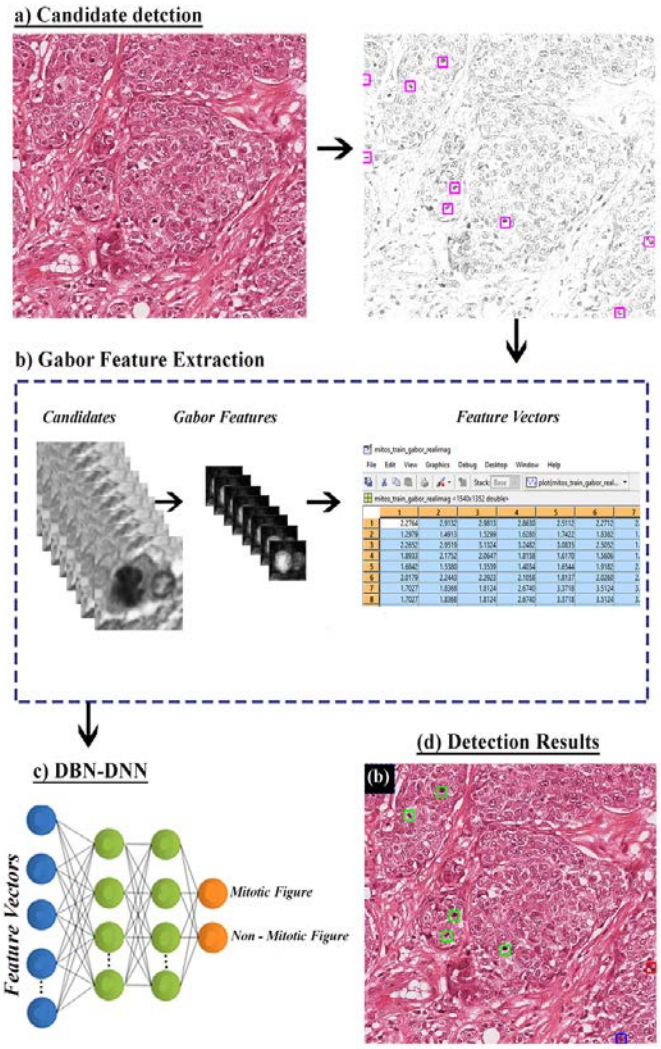

Fig.2. Overview of Methodology (a) Detected candidates marked in pink, (b) Gabor feature extraction, (c) DBN-DNN classification and (d) Detection results: true positives, false positives and false negatives marked in green, red and blue respectively

Each candidate image patches are convolved with a 10×10 complex valued Gabor filters computed for 5 scales and 8 orientations. The filter bank of the 40 filters used is shown in Fig.3. The response of the real part of the filters on a detected candidate object is shown in Fig.4. This results in Gabor feature space with 40 channels of dimensions 80×80. The features are further reduced by applying 3×3 max-pooling on each channel and 1×1×1 max-pooling across the channels resulting in a 26×26 image. The real parts of the image is selected as the features for classification resulting in feature vector of length 26×26 = 656 for each candidate.

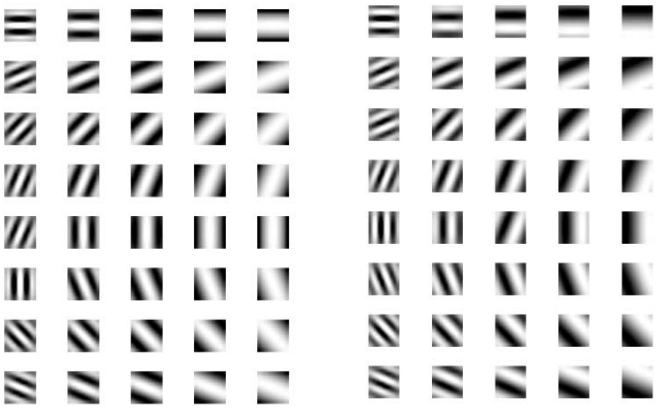

(a) (b)

Fig.3. Gabor Filter bank. (a) real part (b) imaginary part. Rows correspond to different orientations and the columns correspond to different scales

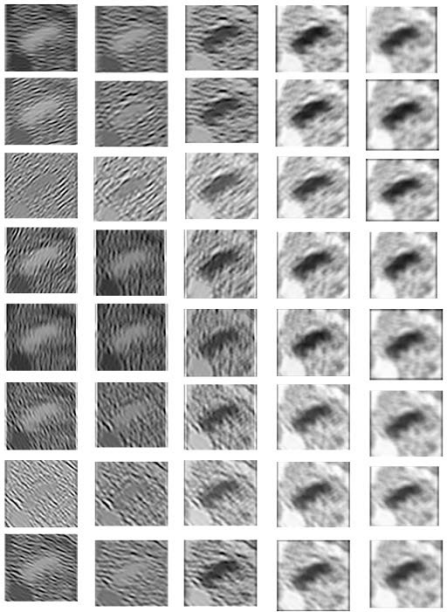

Fig.4. Demonstration of the real part of Gabor filters applied to a candidate object

4.3 CLASSIFICATION USING DEEP NEURAL NETWORKS

A DNN pre-trained via stacked Restricted Boltzmann Machines called as Deep Belief Network-Deep Neural Networks (DBN-DNN) [13, 14] is used to classify the feature vectors of the candidates into one of the two classes: mitotic figure and non-mitotic figure.

4.3.1 Restricted Boltzmann Machines (RBMs):

RBMs are the base units of the DBN-DNN. An RBM is two layer Neural Network: (1) Visible layer (v_1,v_2,...,v_i) (2) Hidden layer (h_1,h_2,....,h_j). Every node of visible layer is connected to every node in hidden layer. There is no intra-layer communication – this is the restriction in a restricted Boltzmann machine. RBMS are trained in a unsupervised manner by many forward and backward passes. In forward pass each visible node takes a low-level feature from an item in the feature set to be learned. In our case, the Gabor feature set has 656 features, so there must be 656 input nodes on the visible layer. At each node in the hidden layer the inputs from the visible layer would combine. Each input is multiplied by a separate weight, the products are summed, added to a bias, and again the result is passed through an activation function to produce the node's output.

The activations of hidden layer become the input in a backward pass. They are multiplied by the same weights. The sum of those products is added to a visible-layer bias at each visible node, and the output of those operations is a reconstruction; i.e. an approximation of the original input. Because the weights of the RBM are randomly initialized, the difference between the reconstructions and the original input is often large. The reconstruction error can be the difference between the values of *r* and the input values, and that error is then back propagated against the RBM's weights, again and again, in an iterative learning process until an error minimum is reached.

In forward pass, an RBM uses inputs to make predictions about node activations $p(h|v;\ w,a,b)$. But on its backward pass, when activations are fed in and guesses about the original data, are computed, an RBM is attempting to estimate the probability of inputs *v* given activations *h*, which are weighted with the same coefficients as those used on the forward pass. This second phase can be expressed as $p(v|h;\ w,b,b)$. Together, those two estimates will lead you to the joint probability distribution of inputs *v* and activations *h* which is $p(v,\ h)$. The Fig.5 shows a restricted Boltzmann machine.

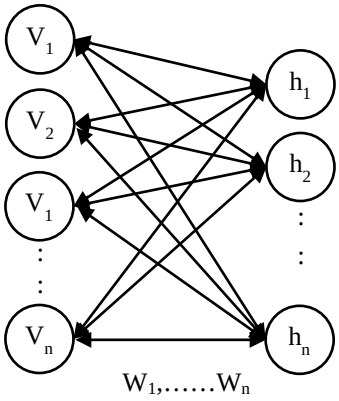

Fig.5. A RBM

The joint probability of neurons in the visible and the hidden layer of the RBM is defined by

$$p(v,h;W,a,b)=\frac{1}{Z}e^{E(v,h;W,a,b)} \tag{2}$$

where, *Z* is the partition function and *E* is the energy function and *T* represents the transpose operator.

$$Z=\sum_{v',h'}e^{E(v',h';W,a,b)} \tag{3}$$

$$E(v,h;W,a,b)=-h^TWv-b^Th-a^Tv \tag{4}$$

The conditional probability of hidden state given the visible state and vice versa are given by

$$p(h=1\,|\,v)=\sigma\left(W^Tv+b\right) \tag{5}$$

$$p(v=1\,|\,h)=\sigma\left(Wh\ +\ c\right) \tag{6}$$

To measure the distance between its estimated probability distribution and the ground-truth distribution of the input, RBMs use Contrastive Divergence Algorithm. The change of parameter *W* using the CD algorithm is given by

$$\Delta w_{ij} = \varepsilon\left(\left\langle v_i^0 h_j^0 \right\rangle - \left\langle v_i^1 h_j^1 \right\rangle\right) \tag{7}$$

where, $\underline{\varepsilon}$ is the learning rate.

In this paper, we apply the inference of RBM proposed by [14].

4.3.2 Deep Belief Networks (DBNs):

A deep belief network (DBN) is formed by stacking RBMs. The states of hidden nodes inferred by the RBM of the first layer are used as input for the second layer. Once the first RBM learns the structure of the input data as it relates to the activations of the first hidden layer, then the data is passed one layer down the net. Now the first hidden layer becomes the visible layer. The activations from the first hidden layer are multiplied by weights at the nodes of the second hidden layer, to produce another set of activations. With every new hidden layer, the weights are adjusted until that layer is able to approximate the input from the previous layer. This is a greedy, layer wise and unsupervised pre-training.

4.3.3 DBN-DNN:

A DBN-DNN is formed by a adding a final decision layer to the DBN. The DBN-DNN is initialized by the prescribed pre-training using the CD algorithm proposed in [14]. Finally a classical back-propagation is applied as supervised learning to fine tune the weights. The output of the (l+1)th layers are given by,

$$q_{l+1} = \sigma\left(W_l^T q_l + b_l\right) \tag{8}$$

The probability of random variable is used as the node output.

$$q_l = P\left(\xi_l = 1\right) = \mathrm{E}_{p(\xi_l=1)}\left[\xi_l\right] \tag{9}$$

The probability (l+1)th node is given by

$$P\left(\xi_{l+1} = 1\right) = \mathrm{E}_{p(\xi_l)}\left(\sigma\left(W_l^T \xi_l + b_l\right)\right) \tag{10}$$

In the back-propagation for the DBN-DNN two sets of derivatives are back propagated as given in [14].

4.3.4 DBN-DNN Mitotic-Figure Classifier:

A 2 hidden layer DBN-DNN with 656-200-50-2 nodes is then constructed. Each instance of the input feature set to the first RBM is a set of Gabor feature vectors extracted from the candidate image patches. The ground truth information (labels) is used in the back propagation algorithm to fine-tune the parameters learned by DBN-DNN.

Table.2. 656-200-50-2 DBN-DNN Mitotic detector

Layer	Type	Neurons
0	Visible (Input Gabor vectors)	656 N
1	Hidden	200 N
2	Hidden	50 N
3	Visible (Output - Mitosis /Non- Mitosis)	2 N

5. RESULTS

The methodology was evaluated on the images of the test set of MITOS dataset and the three slides from the training set of MITOS-ATYPIA dataset. Results were obtained for the images scanned by both scanners: Aperio Scanscope XT and Hamamatsy Nanozoomer 2.0-HT. The performance of the proposed mitotic detection methodology is based on three evaluation metrics namely the precision (*PPV*), the recall (*TPR*) and the *f*1-*score*. The *f-score* = 2 × (*precision* × *recall*)/(*precision* + *recall*) is shown in Table 2. A detected candidate is regarded as a true mitotic figure if its distance is within 8 µm (8 / 0.2455 = 32 pixels for images of scanner Aperio Scanscope XT and 8 / 0.227299 = 35 pixels (horizontal) and 8/0.227531= 35 pixels (vertical) for images of scanner Hamamatsu Nanozoomer 2.0-HT)) from the approximate center of a ground truth mitotic figure. Here True-Positive is the number of mitoses that are ground truth mitoses among the detected mitoses, while False-Positive is the number of mitoses that are not ground truth mitoses among the detected mitoses and False Negatives is the number of ground truth mitoses that have not been detected. The Fig.6 shows the *f-score* of the proposed method on testing it for MITOS valuation dataset in comparison to the first four winning methods in the contest. The classification performance of the constructed DBN-DNN network is evaluated using the root mean square error calculated by

$$rmse = \sqrt{\frac{1}{MN}\sum_{k=1}^{N}\left\| y_k - F(x_k) \right\|_2^2} \tag{11}$$

where, *M* is the number of output classes, *N* is the number of data, x_k represents the *k*-th input data, y_k represents the *k*-th output data. The convergence of the network for root mean square error on the training and testing data of mitos dataset for 1000 iterations is shown in Fig.7. The learning rate was chosen to be 0.8 and the inital momentum was 0.5. The learning rate scale adjustment is 0.01 for every iteration. The Fig.8 shows the mitotic detection results on representative images from the dataset. A closer view of the detection results on sub-images is shown in Fig.9.

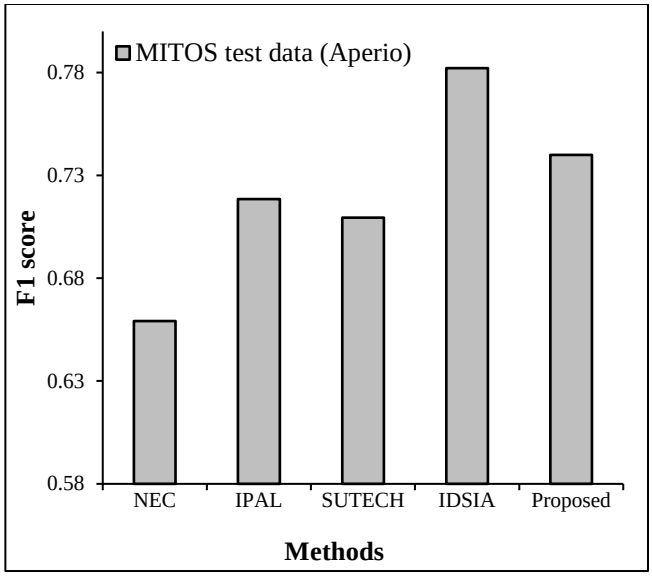

Fig.6. F-measures of various methods for Scanner Aperio images from MITOS dataset

Table.2. Performance Analysis of the proposed method on MITOS and MITOS-ATYPIA dataset

	MITOS Evaluation dataset	MITOS - ATYPIA Training dataset					
		Aperio Scanscope XT			Hamamatsu Nano zoomer 2.0-HT		
		A15	A17	A18	H15	H17	H18
PPV	0.77	0.55	0.62	0.77	0.67	0.62	0.79
TPR	0.72	0.93	0.87	0.71	0.60	0.86	0.83
F-score	0.74	0.69	0.72	0.74	0.71	0.72	0.81

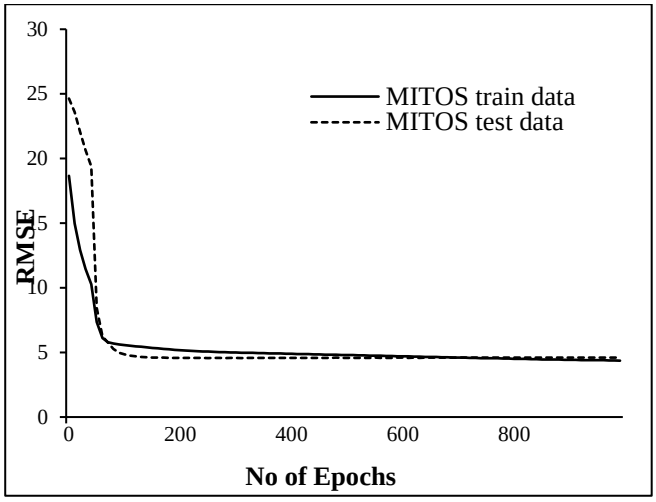

Fig.7. Convergence of training and test data on MITOS dataset

6. CONCLUSION

In light of the persisting need for an objective and reproducible method of assessment of mitotic count in breast cancer images, an efficient automated detection of mitotic figures in H&E stained breast cancer histopathology Images has been presented. The results show that the proposed method is accurate in detecting mitotic figures and worth comparable to the state-of-art methodology proposed by the winning method of MITOS contest. Moreover the method is efficient, scalable and simple to implement compared to the state-of-art method which are computationally expensive and requires immense amount of training data. The next phase of the work aims to validate the methodology on larger datasets to increase performance in automated detection of mitotic figures.

ACKNOWLEDGMENT

The authors would like to acknowledge the involvement and support provided by the DST-FIST computing facility at the Department of Mathematics, Madras Christian College.

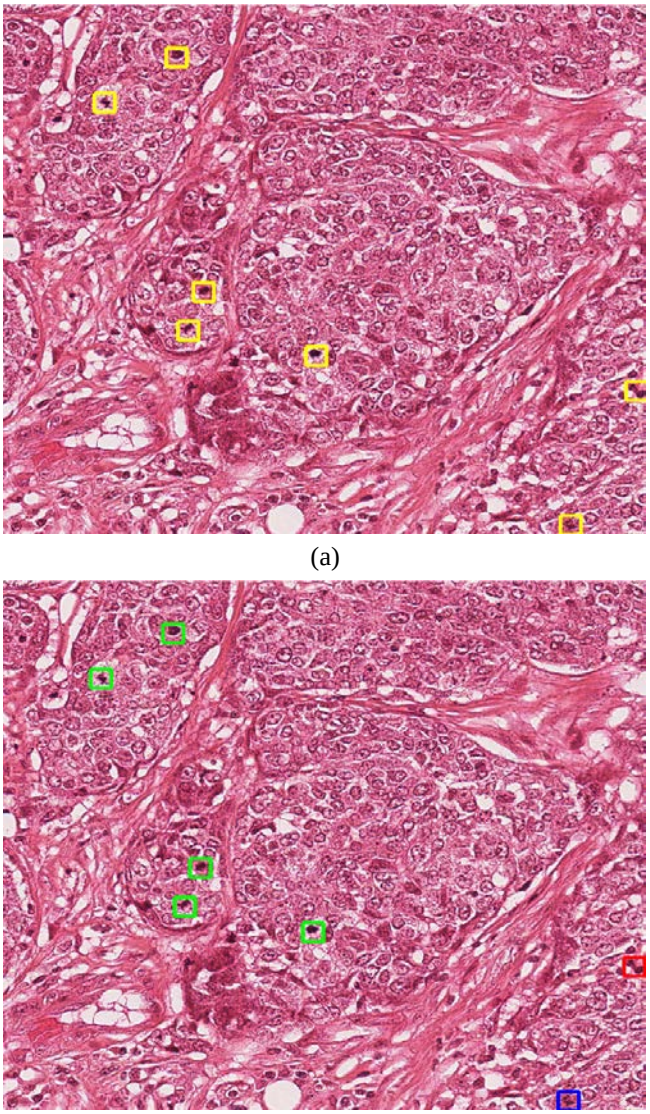

(a)

(b)

Fig.8.(a) Ground truth mitoses marked in yellow, (b) Detection results: true positives, false positives and false negatives marked in red, green and blue respectively

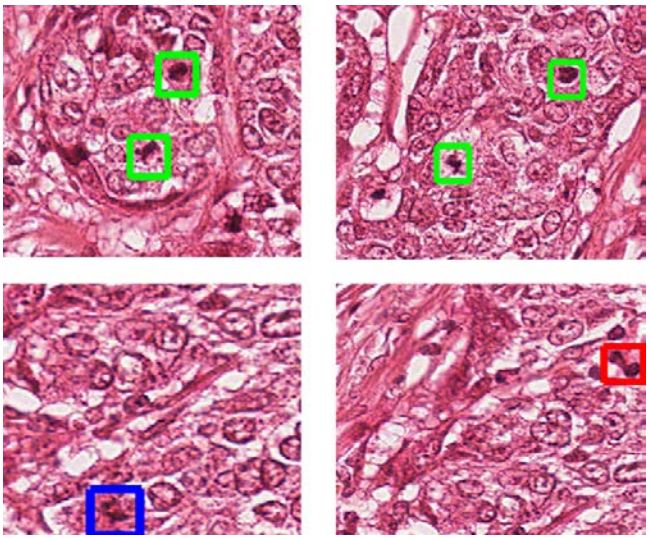

Fig.9. Closer view of the detection results on sub-images

REFERENCES

[1] P.J. Van Diest, E. Van Der Wall, and J.P.A. Baak, "Prognostic Value of Proliferation in Invasive Breast Cancer: A Review", *Journal of Clinical Pathology*, Vol. 57, No. 7, pp. 675-681, 2004.

[2] H.F. Frierson, R.A. Wolber, K.W. Berean, D.W. Franquemont, M.J. Gaffey, J.C. Boyd, and D.C. Wilbur, "Interobserver Reproducibility of the Nottingham Modification of the Bloom and Richardson Histologic Grading Scheme for Infiltrating Ductal Carcinoma", *American Journal of Clinical Pathology*, Vol. 103, No. 2, pp. 195-198, 1995.

[3] L. Roux., D. Racocean., N. Lomenie., M. Kulikova., H. Irshad., J. Klossa., F. Capron., C. Genestie., G.L. Naour and M.N. Gurcan, "Mitosis Detection in Breast Cancer Histological Images", *Journal of Pathology Informatics*, Vol. 4, No. 1, pp. 8-14, 2013.

[4] Mitos and Atypia, "Detection of Mitosis and Evaluation of Nuclear Atypia Score in Breast Cancer Histological Images", *Proceedings of* 22nd *International Conference on Pattern Recognition*, pp. 1-8, 2014.

[5] R.S. Weinstein, A.R. Graham, L.C. Richter, G.P. Barker, E.A. Krupinski, A.M. Lopez, K.A. Erps, A.K. Bhattacharyya, Y. Yagi and J. R. Gilbertson, "Overview of Telepathology, Virtual Microscopy, and Whole Slide Imaging: Prospects for the Future", *Human Pathology*, Vol. 40, No. 8, pp. 1057-1069, 2009.

[6] C.V. Hedvat, "Digital Microscopy: Past, Present, and Future", *Archives of Pathology and Laboratory Medicine*, Vol. 134, No.11, pp. 1666-1670, 2010.

[7] M. Veta, P.J. Van Diest, S.M. Willems, H. Wang, A. Madabhushi, A. Cruz-Roa, F. Gonzalez, A.B.L. Larsen, J.S. Vestergaard, A.B. Dahl, D.C. Cireşan, J. Schmidhuber, A. Giusti, L.M. Gambardella, F.B. Tek, T. Walter, C.W. Wang, S. Kondo, B.J. Matuszewski, F. Precioso, V. Snell, J. Kittler, T.E. De Campos, A.M. Khan, N. M. Rajpoot, E. Arkoumani, M.M. Lacle, M.A. Viergever and J.P.W. Pluim, "Assessment of Algorithms for Mitosis Detection in Breast Cancer Histopathology Images", *Medical Image Analysis*, Vol. 20, No. 1, pp. 237-248, 2015.

[8] D.C. Ciresan., A. Giusti., L.M. Gambardella and J. Schmidhuber., "Mitosis Detection in Breast Cancer Histology Images with Deep Neural Networks", *Proceedings of 16th International Conference on Medical Image Computing and Computer-Assisted Intervention*, pp. 411-418, 2013.

[9] R. C. Gonzalez and R. E. Woods, "*Digital Image Processing*", 3rd Edition, Prentice Hall, 2001.

[10] L. Chengjun and H. Wechsler, "Gabor Feature based Classification using the Enhanced Fisher Linear Discriminant Model for Face Recognition", *IEEE Transactions on Image Processing*, Vol. 11, No. 4, pp.467-476, 2002.

[11] J.K. Kamarainen, V. Kyrki and H. Kalviainen, "Invariance Properties of Gabor Filter-based Features-Overview and Applications", *IEEE Transactions on Image Processing*, vol. 15, No. 5, pp. 1088-1099, 2006.

[12] Mohammad Haghighat, Saman Zonouz and Mohamed Abdel-Mottaleb, "CloudID: Trustworthy Cloud-based and Cross-Enterprise Biometric Identification", *Expert Systems with Applications*, Vol. 42, No. 21, pp. 7905-7916, 2015.

[13] G. Hinton et al., "Deep Neural Networks for Acoustic Modeling in Speech Recognition: The Shared Views of Four Research Groups", *IEEE Signal Processing Magazine*, Vol. 29, No. 6, pp. 82-97, 2012.

[14] M. Tanaka and M. Okutomi, "A Novel Inference of a Restricted Boltzmann Machine", *Proceedings of the 22nd International Conference on Pattern Recognition*, pp. 1526-1531, 2014.